Physics and Imaging in Radiation Oncology 34 (2025) 100746

Contents lists available at ScienceDirect

Physics and Imaging in Radiation Oncology

journal homepage: www.sciencedirect.com/journal/physics-and-imaging-in-radiation-oncology

Original Research Article

Interfractional body surface monitoring using daily cone-beam computed tomography imaging for pediatric adaptive proton therapy☆

Ozgur Ates *, Hoyeon Lee, Jinsoo Uh, Matthew J. Krasin, Thomas E. Merchant, Chia-ho Hua

Department of Radiation Oncology, St. Jude Children's Research Hospital, TN 38105, USA

ARTICLE INFO

Keywords:
Adaptive proton therapy
Pediatric solid tumors
Interfractional body surface changes
Water equivalent path length
CBCT
synthetic CT

ABSTRACT

Background and purpose: A novel method was developed to detect body surface changes on daily cone-beam computed tomography (CBCT) and estimate the impact on proton plan quality for pediatric patients.
Materials and methods: Simulation CT, daily CBCT, and repeat CT images were collected for 21 pediatric non-central nervous system (CNS) patients. Changes in the body surface in the proton beam path ($\Delta Surface_{CBCT}$) were calculated for each spot by comparing simulation CT with daily CBCT. Subsequently, changes in water equivalent path length (WEPL) ($\Delta WEPL_{Synthetic\ CT}$) were calculated for each spot by comparing the simulation CT with the synthetic CT converted from daily CBCT. The ground truth surface ($\Delta Surface_{Repeat\ CT}$) and WEPL changes ($\Delta WEPL_{Repeat\ CT}$) were calculated by comparing the simulation CT with the repeat CT taken on the same day as the CBCT.
Results: The root-mean-square (RMS) error between the $\Delta Surface_{CBCT}$ and $\Delta Surface_{Repeat\ CT}$ was 1.3 mm, while the RMS error between $\Delta WEPL_{Synthetic\ CT}$ and $\Delta WEPL_{Repeat\ CT}$ was 1.6 mm. A strong linear correlation was determined between $\Delta Surface_{CBCT}$ and $\Delta WEPL_{Synthetic\ CT}$ ($R^2 = 0.97$). The non-linear regression analysis of the dose volume parameters indicated that a 5 % decrease in clinical target volume (CTV) D_{min} and $D_{99\%}$ was caused by 3.9 mm and 6.3 mm of $\Delta Surface_{CBCT}$, and 4.0 mm and 6.6 mm of $\Delta WEPL_{Synthetic\ CT}$, respectively.
Conclusions: The findings revealed that a 5 mm change in body surface can lead to a significant degradation of plan quality, reducing CTV D_{min} by 11.7 % and underscoring the need for adapting treatment plan.

1. Introduction

Proton therapy has advantages in cancer treatment, mainly due to its ability to precisely deliver prescribed doses to tumors. These advantages have led to the wide acceptance of proton therapy for the treatment of various cancers [1,2], with promising results in pediatric cancer treatment [3–5]. In pediatric patients, the unique physical properties of protons allow for reduced radiation exposure to healthy tissues, which is critical for minimizing long-term side effects such as growth impairment, neurocognitive deficits, and secondary cancers [5]. This makes proton therapy an invaluable modality in pediatric oncology, where tissue sparing and precision are paramount.

Although proton therapy improves dose sparing to the neighboring healthy tissues with its physical properties, it also makes the dose delivery sensitive to the anatomical changes in patients. Consequently, adaptive proton therapy (APT) has been actively investigated to mitigate the anatomical changes [6–8]. In the APT framework, anatomical variations, such as weight gain/loss, fluid collection, drainage, or tumor regression/progression are detected using cone-beam computed tomography (CBCT) [9,10] or in-room CT [7], and the original proton treatment plan is adapted or new treatment plans are created, to achieve the clinical goals based on the daily anatomical changes. The APT has successfully restored the originally planned dose by accounting for anatomical variations that necessitated the adaptive plan [11–14].

Most studies suggested that the initial plan should be re-evaluated during the course of treatment, typically around week #3 or #4 [14]. Body contour deviation, patient position variations, patient weight changes, and deviations in dose parameters for the target volumes could serve as evaluation criteria [13]. Some studies used machine learning approaches to predict anatomical changes [15] or daily images from

☆ This article is part of a special issue entitled: 'Online and real-time adaptive particle therapy' published in Physics and Imaging in Radiation Oncology.

* Corresponding author.
E-mail addresses: ozgur.ates@stjude.org (O. Ates), hlee01@hku.hk (H. Lee), jinsoo.uh@stjude.org (J. Uh), matthew.krasin@stjude.org (M.J. Krasin), thomas.merchant@stjude.org (T.E. Merchant), chia-ho.hua@stjude.org (C.-h. Hua).

https://doi.org/10.1016/j.phro.2025.100746
Received 17 September 2024; Received in revised form 19 February 2025; Accepted 28 February 2025
Available online 6 March 2025

simulation CT images [16,17] to determine the optimal replanning time or create multiple treatment plans before delivery. However, there is no consensus in quantitative metrics to trigger adaptive workflow [8,18].

In the clinical practice of APT, the evaluation of dose-volume parameters on repeat CT image is commonly used to determine the impact [8]. However, this approach raises concerns, as repeated CT scans may increase the risk of secondary cancer in pediatric patients [19,20]. Additionally, it involves multiple steps, including image data transfer and image registration [21]. Additional artifact correction [22–24] or image synthesis steps [25–28] are required when CBCTs are used for the recalculation of treatment plans.

In this context, the body contour could be used as an indicator of daily tissue discrepancies, which is closely related to changes in the dose distribution in proton therapy for pediatric cancer treatment [14,29] and can be detected from the field of view (FOV) of the daily images. In adaptive photon therapy, it has been shown that body contour deviations larger than 1 cm changes could be used as a criterion to trigger the adaptation workflow [13,30].

The aim of this study was to develop an automated workflow for assessing daily variations in the patient's body surface along the proton beam path using CBCT images of non-central nervous system (CNS) pediatric patients. Additionally, the study aimed to evaluate the relationship between body surface changes and water equivalent path length (WEPL) variations for individual proton spots and to investigate the impact of these variations on plan quality and dose-volume parameters.

2. Materials and methods

2.1. Patient data

Simulation CT, daily CBCT, repeat CT images, and treatment planning datasets—including treatment plans and structure sets—were collected from 21 non-CNS pediatric patients who underwent pencil beam scanning proton therapy. Among these cases, 14 were from a prospective clinical trial (NCT04125095) [31] and 7 were from a retrospective study approved by the Institutional Review Board (IRB). The patient characteristics of the collected data were summarized in Table 1.

Simulation CTs were the initial CT scans of each patient used in proton treatment plan using the treatment planning system (TPS), Eclipse version 16 (Varian Medical Systems, Palo Alto, CA). The collected proton treatment plans comprised of 21 plans including pelvis (n = 16), abdomen (n = 1), thorax (n = 2), extremity (n = 2) sites, and 44 treatment fields. Daily CBCTs were used as image guided radiotherapy (IGRT) purposes obtained for each treatment fraction of the patient setup.

Repeat CTs were acquired during the course of treatment for the purpose of replanning or boost treatment planning. New targets were delineated in the repeat CTs by attending physicians. Daily CBCTs were selected on the same day as the repeat CTs, which served as the ground truth for the validation in this study.

2.2. Spot-based surface calculation

The proposed methods utilized simulation CT images, structure sets, proton treatment plans, and CBCT images as inputs to calculate the surface changes ($\Delta Surface_{CBCT}$) in the proton beam path. During IGRT, the CBCT FOV was guided to ensure that the proton beam path remained within FOV boundaries. During treatment planning, representative beam path structures were created based on 20 % isodose lines to support daily IGRT procedures. This ensures that the CBCT FOV includes the beam path structure to verify possible tissue discrepancies in the beam path.

An automated MIM workflow (MIM Software Inc., Beachwood, OH) was outlined in Fig. 1 for the surface change method. In Fig. 1a, the couch was initially removed, and the body contours were delineated from both the simulation CT and CBCT images using the thresholding method (threshold > -600HU). As a validation, a series of CT and CBCT images from various regions of an anthropomorphic phantom were acquired. External body contours were delineated in both image modalities using an image thresholding tool. It was found that a threshold of >-600 HU accurately represented the body contours in both modalities, with no discernable differences.

The CBCTs were then registered to the simulation CTs using rigid registration based on bony anatomy alignment. In Fig. 1b, the intersection of each proton beam with the simulation and CBCT body surfaces were calculated in an in-house algorithm using MATLAB version 2021a (The MathWorks, Inc., Natick, MA) as a MIM extension based on a MATLAB library [32]. Spot positions, treatment isocenter, gantry and couch angles were obtained from the proton treatment plan (RTPLAN). The intersection point vectors were calculated for both simulation CT and CBCT. Then, the distance between simulation CT and CBCT was computed to determine the ΔSurface for each proton spot. The median ΔSurface was chosen to represent the overall changes in the body surface per treatment field. The positive ΔSurface signified an increase in patient volume (tissue gain), while a negative ΔSurface denoted a reduction (tissue loss).

2.3. Spot-based WEPL calculation

WEPL is defined as the equivalent thickness of water that would cause the same energy loss for a proton as it experiences while traversing a given material. It is commonly used in proton therapy to quantify the effective path length of protons through various tissues based on their relative stopping power (RLSP) [24,33–35]. In this investigation, WEPL was determined for each individual proton spot in a granular level instead of basing calculations on the 2D projection of the target volumes [33–35], as shown in Fig. 1c. This approach prioritized precisely tracking the trajectory of the proton beam itself, while the 2D projection method might dilute the impact of tissue heterogeneity on uncertainties in calculated dose values.

The WEPL for each spot was calculated using Eq. (1), where i denotes the proton spot, dl is the travel length of the proton per voxel (v) calculated by Siddon's method [36], $RLSP(v)$ is the relative stopping power of voxel v. The integration was performed from the proton beam entrance ($l = 0$) to the distal edge of the target volume ($l = d$).

$$WEPL(i) = \int_{l=0}^{l=d} RLSP(v)dl \tag{1}$$

For WEPL calculations, diagnostic CT quality images and a calibration curve are required to convert the Hounsfield Unit (HU) on CT images to the RLSP of protons. Therefore, synthetic CTs were generated from CBCTs (the same day of repeat CT) using a hybrid synthetic CT method [28]. The method combined deformable image registration and cycleGAN to minimize uncertainties in synthetic CT generation. The stoichiometric calibration curve [37], mapping HU to RLSP, was extracted from the Eclipse TPS.

The WEPL was calculated from the simulation CT ($\Delta WEPL_{Simulation\ CT}$) and the synthetic CT ($\Delta WEPL_{Synthetic\ CT}$) for each treatment field using the spot-based method through the distal edge of the clinical target volume (CTV). The new target volumes for the synthetic CTs were rigidly transferred from the repeat CTs. The median of their differences ($WEPL_{Synthetic\ CT} - WEPL_{Simulation\ CT}$) was used to represent WEPL changes ($\Delta WEPL_{Synthetic\ CT}$) for each treatment field. A positive ΔWEPL indicated an increase in patient volume (tissue gain), while a negative ΔWEPL denoted a decrease in patient volume (tissue loss), which is similar to the rationale in $\Delta Surface_{CBCT}$ implementation. The mean and standard deviation (SD) were also calculated for ΔSurface and ΔWEPL values across all patients.

Table 1
Summary of patient characteristics. Abbreviations: RL. Right Lateral, LL. Left Lateral, LPO. Left Posterior Oblique, RPO. Right Posterior Oblique, RAO. Right Anterior Oblique, LAO. Left Anterior Oblique, PA. Posterior-Anterior, AP. Anterior-Posterior, F. Female, M. Male.

Patient number	Diagnosis	Age (Years)	Sex	Disease Site	Beam Arrangements	Prescription (GyRBE) × Fraction	Plan Robustness (setup/range)
1	Rhabdomyosarcoma	1	M	Prostate	RL, LL	1.8 × 20	3 mm/3%
2	Rhabdomyosarcoma	1	M	Bladder/Prostate	LPO, RPO	1.8 × 20	3 mm/3%
3	Rhabdomyosarcoma	2	M	Liver	RAO, RL, RPO	1.8 × 20	5 mm/5%
4	Hepatoblastoma	2	F	Thorax	LPO, RPO	1.8 × 20	3 mm/5%
5	Rhabdomyosarcoma	2	F	Pelvis	PA, RPO	1.8 × 20	5 mm/5%
6	Fibrosarcoma	2	M	Right hip	AP, RL	1.8 × 25	3 mm/3%
7	Rhabdomyosarcoma	7	M	Right pelvis	RL, PA	1.8 × 23	3 mm/3%
8	Rhabdomyosarcoma	7	M	Bladder/Prostate	LPO, RPO, AP	1.8 × 20	3 mm/3%
9	Rhabdomyosarcoma	8	F	Right arm	AP, PA	1.8 × 20	3 mm/3%
10	Ewing's Sarcoma	10	F	Sacrum	LPO, RPO	1.8 × 25	3 mm/3%
11	Ewing's Sarcoma	14	M	Pelvis	PA, RL	1.8 × 25	3 mm/3%
12	Rhabdomyosarcoma	14	M	Prostate	LAO, LPO	1.8 × 20	3 mm/3%
13	Ewing's Sarcoma	15	F	Left pelvis	PA, LAO	1.8 × 25	3 mm/3%
14	Ewing's Sarcoma	16	M	Sacrum	RL, LL	1.8 × 25	3 mm/3%
15	Rhabdomyosarcoma	16	M	Prostate	LPO, RPO	1.8 × 20	3 mm/3%
16	Rhabdomyosarcoma	17	F	Perineum	LPO, RPO	1.8 × 20	3 mm/3%
17	Ewing's Sarcoma	18	M	Right pelvis	RAO, PA	1.8 × 28	5 mm/5%
18	Ewing's Sarcoma	19	M	Thorax	RAO, RPO	1.8 × 25	3 mm/3%
19	Carcinoma	20	F	Right thigh	AP, PA	1.8 × 31	5 mm/3%
20	Rhabdomyosarcoma	20	M	Prostate	RL, LL	1.8 × 20	3 mm/3%
21	Sarcoma	23	M	Left pelvis	PA, LL	1.8 × 31	3 mm/3%

A relationship between the $\Delta Surface_{CBCT}$ and $\Delta WEPL_{Synthetic\ CT}$ was determined using the linear regression method. The $\Delta WEPL_{Synthetic\ CT}$ can therefore be estimated from the $\Delta Surface_{CBCT}$ using this linear association.

2.4. Dose calculation and analysis

The proton convolution superposition (PCS) algorithm in Varian Eclipse (v16.1) that was used in the original plan optimization was employed to recalculate dose on synthetic CT to evaluate changes in minimum dose to the CTV ($\Delta D_{min\ Synthetic\ CT}$) and the dose received by 99 % of the CTV ($\Delta D_{99\%\ Synthetic\ CT}$). The negative correlation between $\Delta D_{min\ Synthetic\ CT}$ and $\Delta D_{99\%\ Synthetic\ CT}$ with respect to $\Delta WEPL_{Synthetic\ CT}$ was analyzed using a non-linear regression technique, which is a mathematical modeling performed to calculate the coefficients *a*, *b*, and *c* of the power function ($y = a \times x^b + c$). The function was selected based on the observed exponential decrease in dose-volume parameters ΔD_{min} and $\Delta D_{99\%}$ with the linear variation in WEPL (ΔWEPL). In this function, *y* represents dose degradations for $\Delta D_{min\ Synthetic\ CT}$ and $\Delta D_{99\%\ Synthetic\ CT}$ and *x* corresponds to $\Delta WEPL_{Synthetic\ CT}$.

2.5. Validation strategies

$\Delta Surface_{CBCT}$ and $\Delta WEPL_{Synthetic\ CT}$ were introduced as two surrogate methods for assessing anatomical changes on the patient's body surface. The repeat CT was deemed representative of the patient's true anatomy. Consequently, changes in the patient's surface changes ($\Delta Surface_{Repeat\ CT}$) and WEPL differences ($\Delta WEPL_{Repeat\ CT}$) were measured using the repeat CT anatomy to confirm findings from CBCT and synthetic CT images. The validations were carried out by calculating root-mean-square (RMS) error and a two-sample Kolmogorov-Smirnov (KS) test between $\Delta Surface_{CBCT}$ and $\Delta Surface_{Repeat\ CT}$, and as well as between $\Delta WEPL_{Synthetic\ CT}$ and $\Delta WEPL_{Repeat\ CT}$. These statistical analyses assessed the statistical similarity between the results obtained from repeat CT and those from CBCT and synthetic CT images. Additionally, the initially planned dose distributions were recalculated on the repeat CTs as verification plans using PCS algorithm in Varian Eclipse (v16.1) to determine the ground truth dose volume parameters, namely $\Delta D_{min\ Repeat\ CT}$, and $\Delta D_{99\%\ Repeat\ CT}$.

3. Results

3.1. Validation procedure

Spot-based body surface changes on CBCT anatomy ($\Delta Surface_{CBCT}$) and WEPL differences in synthetic CT ($\Delta WEPL_{Synthetic\ CT}$) were individually validated against repeat CT anatomy for each ground truth method ($\Delta Surface_{Repeat\ CT}$ and $\Delta WEPL_{Repeat\ CT}$) as shown in Fig. 2. The linear regression technique revealed the strong correlations of $R^2 = 0.84$ and $R^2 = 0.86$ for the determinations of ΔSurface in Fig. 2a and ΔWEPL in Fig. 2b, respectively. The RMS error between $\Delta Surface_{CBCT}$ and $\Delta Surface_{Repeat\ CT}$ was found to be 1.3 mm, while the RMS error between $\Delta WEPL_{Synthetic\ CT}$ and $\Delta WEPL_{Repeat\ CT}$ was 1.6 mm. These findings bolstered confidence in the accuracy of the methods relative to the true anatomy as depicted by repeat CT. Furthermore, the two-sample Kolmogorov-Smirnov test showed no statistically significant differences between $\Delta Surface_{CBCT}$ and $\Delta Surface_{Repeat\ CT}$ as well as between $\Delta WEPL_{Synthetic\ CT}$ and $\Delta WEPL_{Repeat\ CT}$, with high p-values of 0.99 and 0.60, respectively.

In Fig. 3a, ΔSurface was evaluated against ΔWEPL for repeat CT relative to simulation CT, demonstrating an excellent agreement ($R^2 = 0.97$) between ΔSurface and ΔWEPL methods. Similarly, as depicted in Fig. 3b, $\Delta Surface_{CBCT}$ was compared with $\Delta WEPL_{Synthetic\ CT}$ against simulation CT, confirming a high correlation ($R^2 = 0.97$) between these methods. The comparison between $\Delta Surface_{CBCT}$ and $\Delta WEPL_{Repeat\ CT}$ also showed a strong linear correlation ($R^2 = 0.84$), as shown in Fig. 3c.

3.2. Dose distribution analysis

Table 2 summarized the results of $\Delta Surface_{CBCT}$, $\Delta Surface_{Repeat\ CT}$, $\Delta WEPL_{Synthetic\ CT}$, and $\Delta WEPL_{Repeat\ CT}$ for each of 44 treatment fields, and also dose volume parameters for all 21 patients.

The mean and SD values, calculated across all patients, were 2.4 mm ± 2.1 mm for $\Delta Surface_{CBCT}$ and 2.3 mm ± 1.8 mm for $\Delta Surface_{Repeat\ CT}$. Similarly, $\Delta WEPL_{Synthetic\ CT}$ had a mean and SD of 2.9 mm ± 2.4 mm, while $\Delta WEPL_{Repeat\ CT}$ was 2.5 mm ± 1.9 mm.

The dose volume parameters of ΔD_{min} and $\Delta D_{99\%}$ representing the drop in CTV target coverage calculated as a difference from simulation CT to repeat CT and synthetic CT images in verification plans revealed the impact of daily WEPL variations in the daily plan quality. The CTV $\Delta D_{min\ Repeat\ CT}$ had mean and SD coverage decline of 13.6 % ±28 %,

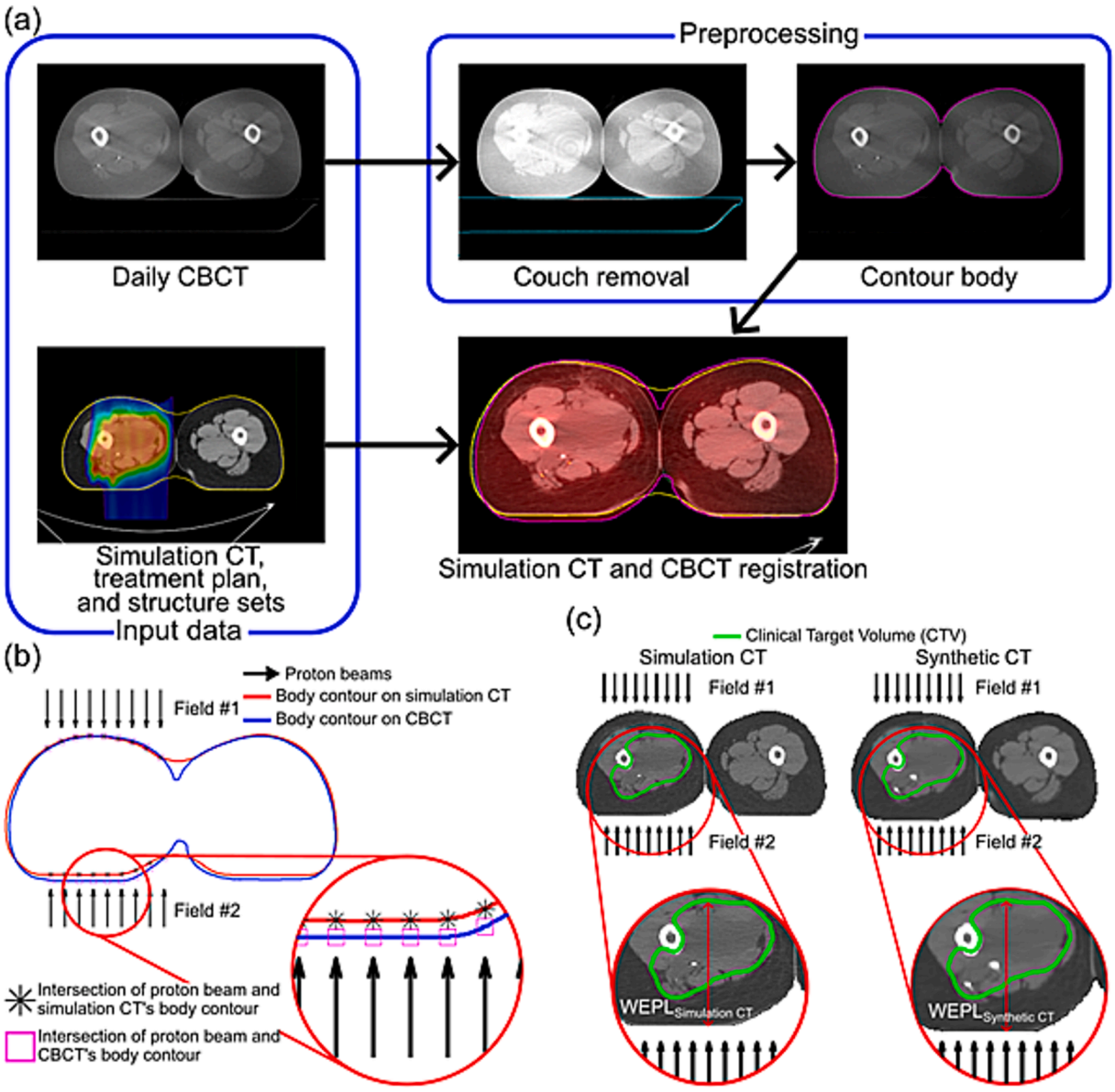

Fig. 1. (a) Workflow illustrates the input of simulation CT, proton treatment planning datasets, and CBCT. Preprocessing includes removal of the treatment couch from CBCT and delineation of the body surface contour, followed by a registration of simulation CT and CBCT using rigid registration. (b) Illustration of the spot-based surface change calculation method ($\Delta Surface_{CBCT}$). (c) Illustration of the spot-based WEPL calculation method ($\Delta WEPL_{Synthetic\ CT}$).

while CTV $\Delta D_{min\ Synthetic\ CT}$ had mean and SD coverage reduction of 15.9 % ±27.5 %. Similarly, CTV $\Delta D_{99\%\ Repeat\ CT}$ had a mean coverage loss of 7.8 % ±20.8 %, whereas CTV $\Delta D_{99\%\ Synthetic\ CT}$ had mean and SD coverage decrease of 4.3 % ±8.7 %.

The largest changes of ΔSurface ($\Delta Surface_{Repeat\ CT}$ = 9.1 mm and $\Delta Surface_{CBCT}$ = 8.3 mm) and ΔWEPL ($\Delta WEPL_{Repeat\ CT}$ = 9.0 mm and $\Delta WEPL_{Synthetic\ CT}$ = 8.9 mm) were observed for patient #17 and field #1. These changes accounted for 89.3 % decline in CTV ΔD_{min} when recalculated in verification plans of both repeat CT and synthetic CT.

In seeking a mathematical relationship between ΔWEPL and dose volume parameters, strong correlations emerged between these two variables, which were formulated using a power law relationship and established through non-linear regression, as shown in Fig. 4a–d. High R^2 values, used as a variable for goodness of fit enabled the model to accurately predict dose volume parameters or the decline in target coverage based on ΔWEPL deviations within the data range used to generate the model. Strong correlations were observed between $\Delta WEPL_{Repeat\ CT}$ and CTV $\Delta D_{min\ Repeat\ CT}$ (R^2 = 0.90) as well as $\Delta WEPL_{Repeat\ CT}$ and CTV $\Delta D_{99\%\ Repeat\ CT}$ (R^2 = 0.88), as shown in Fig. 4a and b, respectively. Similarity, as presented in Fig. 4c and d, robust correlations were also demonstrated between $\Delta WEPL_{Synthetic\ CT}$ and CTV $\Delta D_{min\ Synthetic\ CT}$ (R^2 = 0.84), and between $\Delta WEPL_{Synthetic\ CT}$ and CTV $\Delta D_{99\%\ Synthetic\ CT}$ (R^2 = 0.89). The non-linear regression analysis revealed that a 5 % decrease in CTV D_{min} and $D_{99\%}$ was caused by 4.0 mm and 6.6 mm in $\Delta WEPL_{Synthetic\ CT}$ and 3.4 mm and 6.9 mm in $\Delta WEPL_{Repeat\ CT}$, respectively. The relationship also indicated that a decrease of >2.5 % occurred in CTV D_{min} when ΔWEPL exceeded 3 mm on both repeat CT and synthetic CT images.

Owing to the linear relationship established between ΔWEPL and ΔSurface in Fig. 3, dose-volume parameter variations can be estimated from ΔSurface. Non-linear regression revealed strong power law relationships between ΔSurface and dose-volume parameters, as shown in Fig. 4e–h. Strong correlations were observed between $\Delta Surface_{Repeat\ CT}$ and CTV $\Delta D_{min\ Repeat\ CT}$ (R^2 = 0.91) as well as $\Delta Surface_{Repeat\ CT}$ and CTV $\Delta D_{99\%\ Repeat\ CT}$ (R^2 = 0.89), as shown in Fig. 4e and f, respectively. Fig. 4g and h demonstrated robust correlation between $\Delta Surface_{CBCT}$

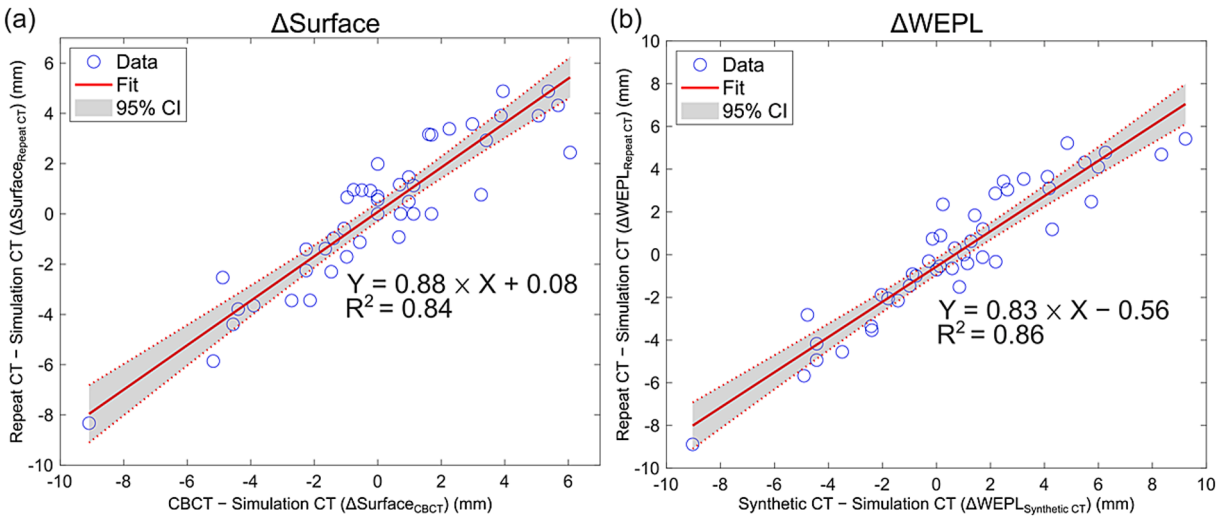

Fig. 2. (a) ΔSurface and (b) ΔWEPL results from the CBCT and synthetic CT when compared to repeat CT.

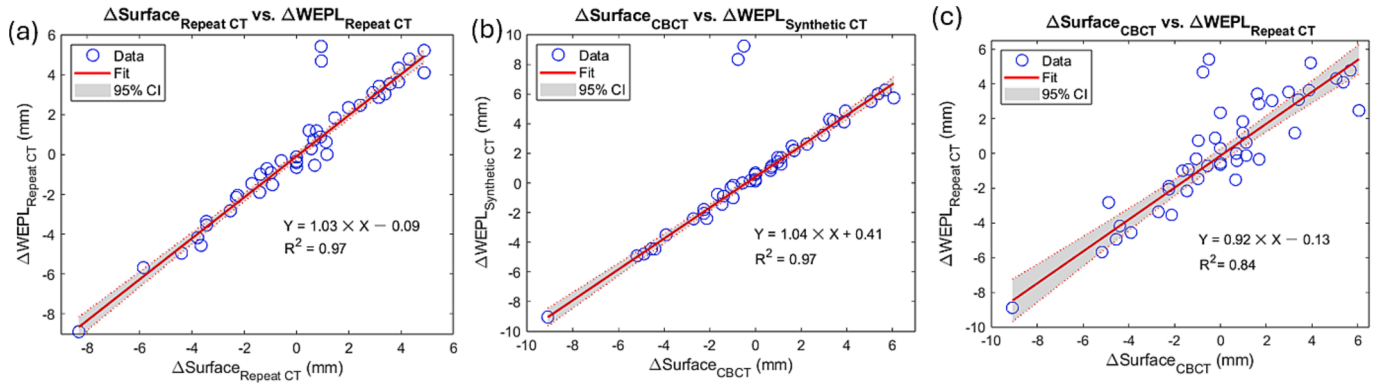

Fig. 3. Comparisons of ΔSurface vs. ΔWEPL for (a), $\Delta Surface_{Repeat\ CT}$ vs. $\Delta WEPL_{Repeat\ CT}$ and (b) $\Delta Surface_{CBCT}$ vs. $\Delta WEPL_{Synthetic\ CT}$, (c) A comparison of $\Delta Surface_{CBCT}$ vs. $\Delta WEPL_{Repeat\ CT}$.

and CTV $\Delta D_{min\ Synthetic\ CT}$ ($R^2 = 0.87$) and between $\Delta Surface_{CBCT}$ and CTV $\Delta D_{99\%\ Synthetic\ CT}$ ($R^2 = 0.79$). The trend analysis showed that a 5 % decrease in CTV D_{min} and D_{99} was caused by 3.9 mm and 6.3 mm in $\Delta Surface_{CBCT}$ and 3.2 mm and 5.9 mm in $\Delta Surface_{Repeat\ CT}$ respectively. The relationship also indicated that a decrease of > 3.5 % occurred in CTV D_{min} when ΔSurface exceeded 3.5 mm on both repeat CT and synthetic CT images.

4. Discussion

Daily tissue discrepancies can serve as anatomical markers which assist clinicians to predict the impact on the daily plan quality. Several studies highlighted the use of $D_{98\%}$, $D_{99\%}$, and D_{min} as critical parameters for assessing the quality of proton therapy plans [9,10,12,30,34]. Consequently, estimating dose volume parameters from ΔSurface and ΔWEPL streamlines the decision-making process in adaptive proton therapy. The proposed method estimates the consequences on the dose distribution directly from daily CBCT images without requiring diagnostic-quality imaging or additional processing steps such as data transfer, image correction, synthetic CT generation [25,26,38–40], or deformable image registration [26,41,42]. These steps are typically required for dosimetric evaluation in repeated imaging, a common practice in adaptive proton therapy [8]. In the proposed methods, ΔWEPL was evaluated for each proton spot and estimated the impact on the dose coverage of the CTV. Existing studies analyzed ΔWEPL from the 2D projection of the CTV by means of validating the image quality of scatter-corrected CBCT [43], and synthetic CT generated from CBCT [28,44]. However, these studies have not focused on monitoring inter-fractional tissue changes and their association with changes in the dose distribution in proton therapy.

The proposed methods effectively detected external body surface changes using a novel spot-based body surface change calculation and helped assess their impact on dose distributions. However, the method cannot detect internal density changes, which led to the outliers observed in Fig. 3. As one of the outliers, a patient exhibited significant ΔWEPL due to heart volume changes on the simulation CT, repeat CT, and CBCT, which introduced, despite only minor deviation in ΔSurface. Therefore, the proposed methods may not accurately estimate dosimetric consequences for the disease sites affected by internal organ motion [45] or density changes (e.g., bowel gas) [35,46]. Further investigation is needed to incorporate the internal density changes into the methods to improve the plan robustness, as the robustness depends on various factors such as the size and depth of the target, heterogeneity along the beam path, and the field margin for spot placements.

Accurate representation of body contours in both CT and daily CBCT is crucial for this approach. Due to image noise in CBCTs, image thresholding tools should be used carefully, with visual inspections to ensure accuracy. A similar phantom validation, as described in Section 2.2, could be performed for the same anatomy in both CT and CBCT images. However, a limitation of this study is that the surface change and WEPL methods were not designed for images with artifacts, such as metal implants or beam hardening, in the beam path.

Table 2
Summary of ΔSurface, ΔWEPL, and dose volume parameters of target volumes.

Patient number	Field number	CBCT/Synthetic CT – Simulation CT (mm)		Repeat CT – Simulation CT (mm)		Verification Plans for CTV D_{min} (%)	Verification Plans for CTV $D_{99\%}$ (%)
		$\Delta Surface_{CBCT}$	$\Delta WEPL_{Synthetic\ CT}$	$\Delta Surface_{Repeat\ CT}$	$\Delta WEPL_{Repeat\ CT}$	Simulation CT / Repeat CT / Synthetic CT	Simulation CT /Repeat CT / Synthetic CT
1	1	−1.5	−1.4	−2.3	−2.2	94.8 / 94.6 / 94.1	96.1 / 95.8 / 95.7
	2	−2.1	−2.4	−3.4	−3.5		
2	1	1.1	1.7	0.0	−0.1	94.1 / 94.1 / 94.1	95.1 / 95.1 / 95.2
	2	1.7	2.2	0.0	−0.3		
3	1	0.0	0.1	0.7	−0.5	96.3 / 97.3 / 97.6	98.9 / 98.9 / 98.8
	2	0.0	0.6	0.0	−0.7		
	3	0.7	1.0	1.2	0.0		
4	1	−0.5	9.2	0.9	5.4	93.1 / 88.3 / 70.9	94.6 / 93.3 / 84.5
	2	−0.8	8.3	1.0	4.7		
5	1	−1.4	−0.9	−1.0	−0.9	99.3 / 97.3 / 98.6	100.7 / 100.1 / 100.3
	2	−0.6	0.0	−1.1	−0.7		
6	1	−2.7	−2.4	−3.5	−3.4	93.5 / 7.4 / 14.7	95.9 / 88.3 / 90.4
	2	−5.2	−4.9	−5.9	−5.7		
7	1	3.9	4.9	4.9	5.2	91.0 / 68.5 /69.5	95.4 / 84.5 / 85.0
	2	1.0	1.7	0.5	1.2		
8	1	−2.3	−1.8	−2.3	−2.1	96.5 / 92.7 / 92.7	98.5 / 98.0 / 98.4
	2	−2.3	−2.0	−1.4	−1.9		
	3	−1.0	−1.0	−1.7	−1.5		
9	1	5.1	5.5	3.9	4.3	89.9 / 79.7 / 70.5	95.1 / 90.0 / 87.7
	2	3.3	4.3	0.8	1.2		
10	1	1.7	2.2	3.2	2.9	90.6 / 90.6 / 85.7	97.2 / 97.0 / 97.1
	2	2.3	2.6	3.4	3.0		
11	1	−4.9	−4.8	−2.5	−2.8	92.3 / 92.0 / 90.9	94.3 / 94.1 / 93.8
	2	0.7	1.2	0.0	−0.4	97.1 / 96.8 / 96.2	98.1 / 97.9 / 97.7
12	1	−1.1	−0.3	−0.6	−0.3	92.9 / 90.2 / 92.2	94.5 / 93.8 / 94.3
	2	−1.7	−0.8	−1.4	−1.0		
13	1	1.0	1.4	1.5	1.8	81.9 / 29.2 / 26.8	96.0 / 86.7 / 84.1
	2	5.7	6.3	4.3	4.8		
14	1	0.0	0.7	0.6	0.3	98.5 / 98.5 / 98.2	101.2 / 101.4 / 101.2
	2	1.1	1.3	1.1	0.6		
15	1	3.4	4.2	2.9	3.1	92.0 / 92.3 / 92.2	93.1 / 93.4 / 93.4
	2	3.9	4.1	3.9	3.6		
16	1	3.0	3.2	3.6	3.5	96.5 / 89.5 / 93.4	98.6 / 98.3 / 98.3
	2	0.0	0.2	2.0	2.4		
17	1	−9.1	−9.0	−8.3	−8.9	89.3 / 19.9 / 31.7	100.2 / 86.8 / 92.3
	2	0.7	0.9	−0.9	−1.5		
18	1	−1.0	−0.2	0.7	0.7	52.8 / 61.0 / 44.9	96.9 / 97.1 / 97.8
	2	1.6	2.5	3.2	3.4		
19	1	−0.2	0.2	0.9	0.9	88.4 / 85.3 / 79.2	93.8 / 93.3 / 88.6
	2	6.1	5.7	2.4	2.5		
20	1	−4.6	−4.4	−4.4	−4.9	96.5 / 94.1 / 93.6	98.6 / 98.3 / 98.7
	2	−3.9	−3.5	−3.7	−4.6		
21	1	5.4	6.0	4.9	4.1	93.6 / 80.7 / 79.9	99.4 / 94.3 / 94.7
	2	−4.4	−4.4	−3.8	−4.2		

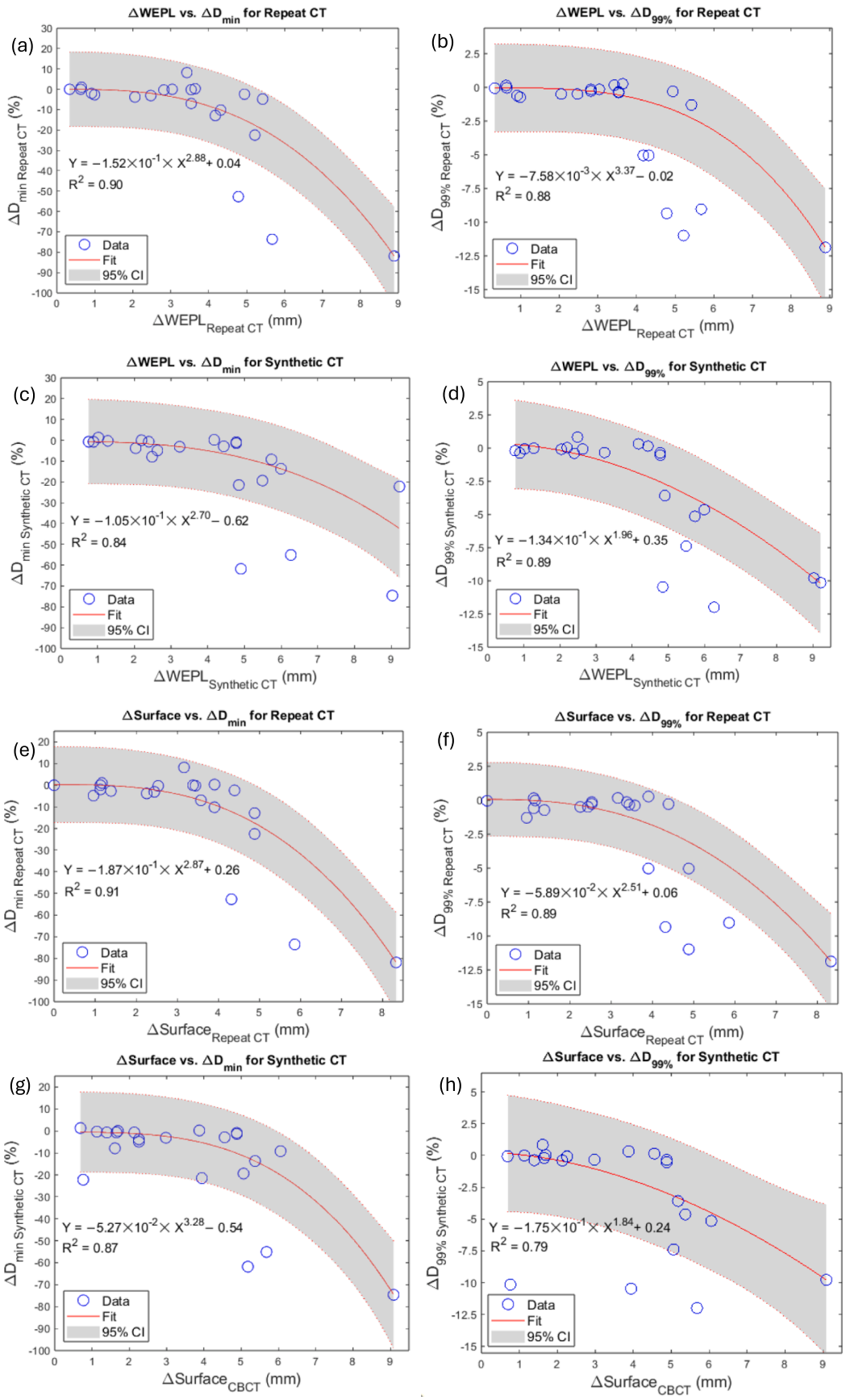

Fig. 4. Relationships between ΔWEPL and dose volume parameters of CTV for repeat CT in (a, b) and synthetic CT in (c, d). Relationships between ΔSurface and dose volume parameters of CTV for repeat CT in (e, f) and synthetic CT/CBCT in (g, h).

Moreover, another limitation of the study is the considerable uncertainties in the coefficients of the power law relationship between ΔWEPL and calculated dose values. This issue arises mainly due to the inclusion of patients with various disease sites in the analysis. While this study serves as a proof of concept for our methods, future work will focus on a dedicated cohort with a similar disease site, target size and planning parameters, thereby enhancing the precision of the relationship.

CRediT authorship contribution statement

Ozgur Ates: Conceptualization, Validation, Visualization, Supervision, Formal analysis, Writing – original draft. **Hoyeon Lee:** Formal analysis, Software, Validation, Methodology, Writing – original draft. **Jinsoo Uh:** Software, Methodology, Writing – review & editing. **Matthew J. Krasin:** Project administration, Supervision, Writing – review & editing. **Thomas E. Merchant:** Project administration, Resources, Writing – review & editing. **Chia-ho Hua:** Project administration, Resources, Writing – review & editing.

Declaration of competing interest

The authors declare that they have no known competing financial interests or personal relationships that could have appeared to influence the work reported in this paper.

Acknowledgment

The authors thank the Department of Radiation Oncology at St. Jude Children's Research Hospital, and American Lebanese Syrian Associated Charities (ALSAC) in Memphis, TN.

References

[1] Mohan R, Grosshans D. Proton therapy – Present and future. Adv Drug Deliver Rev 2017;109:26–44. https://doi.org/10.1016/j.addr.2016.11.006.
[2] Brada M, Pijls-Johannesma M, Ruysscher DD. Current clinical evidence for proton therapy. Cancer J 2009;15:319–24. https://doi.org/10.1097/ppo.0b013e3181b6127c.
[3] Hill-Kayser CE, Tochner Z, Li Y, Kurtz G, Lustig RA, James P, et al. Outcomes after proton therapy for treatment of pediatric high-risk neuroblastoma. Int J Radiat Oncol Biol Phys 2019;104:401–8. https://doi.org/10.1016/j.ijrobp.2019.01.095.
[4] Indelicato DJ, Rotondo RL, Uezono H, Sandler ES, Aldana PR, Ranalli NJ, et al. Outcomes following proton therapy for pediatric low-grade glioma. Int J Radiat Oncol Biol Phys 2019;104:149–56. https://doi.org/10.1016/j.ijrobp.2019.01.078.
[5] Thomas H, Timmermann B. Paediatric proton therapy. Br J Radiol 2019;93:20190601. https://doi.org/10.1259/bjr.20190601.
[6] Paganetti H, Botas P, Sharp GC, Winey B. Adaptive proton therapy. Phys Med Biol 2021;66:22TR01. https://doi.org/10.1088/1361-6560/ac344f.
[7] Albertini F, Matter M, Nenoff L, Zhang Y, Lomax A. Online daily adaptive proton therapy. Br J Radiol 2019;93:20190594. https://doi.org/10.1259/bjr.20190594.
[8] Trnkova P, Zhang Y, Toshito T, Heijmen B, Richter C, Aznar MC, et al. A survey of practice patterns for adaptive particle therapy for interfractional changes. Phys Imaging Radiat Oncol 2023;26:100442. https://doi.org/10.1016/j.phro.2023.100442.
[9] Bobić M, Lalonde A, Sharp GC, Grassberger C, Verburg JM, Winey BA, et al. Comparison of weekly and daily online adaptation for head and neck intensity-modulated proton therapy. Phys Med Bio 2021;66:055023. https://doi.org/10.1088/1361-6560/abe050.
[10] Botas P, Kim J, Winey B, Paganetti H. Online adaption approaches for intensity modulated proton therapy for head and neck patients based on cone beam CTs and Monte Carlo simulations. Phys Med Biol 2018;64:015004. https://doi.org/10.1088/1361-6560/aaf30b.
[11] Huiskes M, Astreinidou E, Kong W, Breedveld S, Heijmen B, Rasch C. Dosimetric impact of adaptive proton therapy in head and neck cancer – A review. Clin Transl Radiat Oncol 2023;39:100598. https://doi.org/10.1016/j.ctro.2023.100598.
[12] Tamura H, Kobashi K, Nishioka K, Yoshimura T, Hashimoto T, Shimizu S, et al. Dosimetric advantages of daily adaptive strategy in IMPT for high-risk prostate cancer. J Appl Clin Med Phys 2022;23:e13531. https://doi.org/10.1002/acm2.13531.
[13] Avgousti R, Antypas C, Armpilia C, Simopoulou F, Liakouli Z, Karaiskos P, et al. Adaptive radiation therapy: when, how and what are the benefits that literature provides? Cancer Radiother 2022;26:622–36. https://doi.org/10.1016/j.canrad.2021.08.023.
[14] Uh J, Jordan JA, Pappo AS, Krasin MJ, Hua C. Adaptive proton therapy for pediatric parameningeal rhabdomyosarcoma: on-treatment anatomic changes and timing to replanning. Clin Oncol 2023;35:245–54. https://doi.org/10.1016/j.clon.2023.01.013.
[15] Iliadou V, Kakkos I, Karaiskos P, Kouloulias V, Platoni K, Zygogianni A, et al. Early prediction of planning adaptation requirement indication due to volumetric alterations in head and neck cancer radiotherapy: a machine learning approach. Cancers 2022;14:3573. https://doi.org/10.3390/cancers14153573.
[16] Lee D, Hu Y, Kuo L, Alam S, Yorke E, Li A, et al. Deep learning driven predictive treatment planning for adaptive radiotherapy of lung cancer. Radiother Oncol 2022. https://doi.org/10.1016/j.radonc.2022.02.013.
[17] Zhang Y, Holloway SM, Wilson MZ, Alshaikhi J, Tan W, Royle G, et al. DIR-based models to predict weekly anatomical changes in head and neck cancer proton therapy. Phys Med Biol 2022;67:095001. https://doi.org/10.1088/1361-6560/ac5fe2.
[18] Green OL, Henke LE, Hugo GD. Practical clinical workflows for online and offline adaptive radiation therapy. Semin Radiat Oncol 2019;29:219–27. https://doi.org/10.1016/j.semradonc.2019.02.004.
[19] Huang R, Liu X, He L, Zhou P-K. Radiation exposure associated with computed tomography in childhood and the subsequent risk of cancer: a meta-analysis of cohort studies. Dose-Response 2020;18:1559325820923828. https://doi.org/10.1177/1559325820923828.
[20] Pearce MS, Salotti JA, Little MP, McHugh K, Lee C, Kim KP, et al. Radiation exposure from CT scans in childhood and subsequent risk of leukaemia and brain tumours: a retrospective cohort study. Lancet 2012;380:499–505. https://doi.org/10.1016/s0140-6736(12)60815-0.
[21] Deiter N, Chu F, Lenards N, Hunzeker A, Lang K, Mundy D. Evaluation of replanning in intensity-modulated proton therapy for oropharyngeal cancer: factors influencing plan robustness. Med Dosim 2021;45:384–92. https://doi.org/10.1016/j.meddos.2020.06.002.
[22] Lalonde A, Winey B, Verburg J, Paganetti H, Sharp GC. Evaluation of CBCT scatter correction using deep convolutional neural networks for head and neck adaptive proton therapy. Phys Med Biol 2020;65:245022. https://doi.org/10.1088/1361-6560/ab9fcb.
[23] Park Y, Sharp GC, Phillips J, Winey BA. Proton dose calculation on scatter-corrected CBCT image: feasibility study for adaptive proton therapy. Med Phys 2015;42:4449–59. https://doi.org/10.1118/1.4923179.
[24] Andersen AG, Park Y-K, Elstrøm UV, Petersen JBB, Sharp GC, Winey B, et al. Evaluation of an a priori scatter correction algorithm for cone-beam computed tomography based range and dose calculations in proton therapy. Phys Imaging Radiat Oncol 2020;16:89–94. https://doi.org/10.1016/j.phro.2020.09.014.
[25] Xu Y, Jin W, Butkus M, Ornelas MD, Cyriac J, Studenski MT, et al. Cone beam CT-based adaptive intensity modulated proton therapy assessment using automated planning for head-and-neck cancer. Radiat Oncol 2024;19:13. https://doi.org/10.1186/s13014-024-02406-9.
[26] Thummerer A, Zaffino P, Meijers A, Marmitt GG, Seco J, Steenbakkers RJHM, et al. Comparison of CBCT based synthetic CT methods suitable for proton dose calculations in adaptive proton therapy. Phys Med Biol 2020;65:095002. https://doi.org/10.1088/1361-6560/ab7d54.
[27] Wynne JF, Lei Y, Pan S, Wang T, Roper JR, Patel PR, et al. Rapid unpaired CBCT-based synthetic CT for CBCT-guided adaptive radiotherapy. Int J Radiat Oncol Biol Phys 2023;117:S179. https://doi.org/10.1016/j.ijrobp.2023.06.2524.
[28] Uh J, Wang C, Jordan JA, Pirlepesov F, Becksfort JB, Ates O, et al. A hybrid method of correcting CBCT for proton range estimation with deep learning and deformable image registration. Phys Med Biol 2023;68:165004. https://doi.org/10.1088/1361-6560/ace754.
[29] Mannina E, Bartlett G, Wallace D, McMullen K. Steroid-induced adaptive proton planning in a pediatric patient with low grade glioma: a case report and literature review. Pr Radiat Oncol 2014;4:50–4. https://doi.org/10.1016/j.prro.2013.06.002.
[30] Weppler S, Quon H, Banerjee R, Schinkel C, Smith W. Framework for the quantitative assessment of adaptive radiation therapy protocols. J Appl Clin Med Phys 2018;19:26–34. https://doi.org/10.1002/acm2.12437.
[31] Estimating Setup Uncertainty in Pediatric Proton Therapy Using Volumetric Images 2020. https://classic.clinicaltrials.gov/ct2/show/NCT04125095 (accessed June 14, 2024).
[32] Schwarz DM. Fast and Robust Curve Intersections 2017. https://www.mathworks.com/matlabcentral/fileexchange/11837-fast-and-robust-curve-intersections (accessed June 14, 2024).
[33] Kim J, Park Y-K, Sharp G, Busse P, Winey B. Water equivalent path length calculations using scatter-corrected head and neck CBCT images to evaluate patients for adaptive proton therapy. Phys Med Biol 2017;62:59–72. https://doi.org/10.1088/1361-6560/62/1/59.
[34] Ates O, Uh J, Pirlepesov F, Hua C-H, Merchant TE, Krasin MJ. Monitoring of interfractional proton range verification and dosimetric impact based on daily CBCT for pediatric patients with pelvic tumors. Cancers 2023;15:4200. https://doi.org/10.3390/cancers15174200.
[35] Narita Y, Kato T, Takemasa K, Sato H, Ikeda T, Harada T, et al. Dosimetric impact of simulated changes in large bowel content during proton therapy with simultaneous integrated boost for locally advanced pancreatic cancer. J Appl Clin Med Phys 2021;22:90–8. https://doi.org/10.1002/acm2.13429.
[36] Siddon RL. Fast calculation of the exact radiological path for a three-dimensional CT array. Med Phys 1985;12(252):255. https://doi.org/10.1118/1.595715.
[37] Schneider U, Pedroni E, Lomax A. The calibration of CT Hounsfield units for radiotherapy treatment planning. Phys Med Biol 1996;41:111–24. https://doi.org/10.1088/0031-9155/41/1/009.
[38] Bäumer C, Frakulli R, Kohl J, Nagaraja S, Steinmeier T, Worawongsakul R, et al. Adaptive proton therapy of pediatric head and neck cases using MRI-based

synthetic CTs: initial experience of the prospective KiAPT study. Cancers 2022;14:2616. https://doi.org/10.3390/cancers14112616.

[39] Taasti VT, Hattu D, Peeters S, van der Salm A, van Loon J, de Ruysscher D, et al. Clinical evaluation of synthetic computed tomography methods in adaptive proton therapy of lung cancer patients. Phys Imaging Radiat Oncol 2023;27:100459. https://doi.org/10.1016/j.phro.2023.100459.

[40] Gao L, Xie K, Wu X, Lu Z, Li C, Sun J, et al. Generating synthetic CT from low-dose cone-beam CT by using generative adversarial networks for adaptive radiotherapy. Radiat Oncol 2021;16:202. https://doi.org/10.1186/s13014-021-01928-w.

[41] Stanforth A, Lin L, Beitler JJ, Janopaul-Naylor JR, Chang C, Press RH, et al. Onboard cone-beam CT-based replan evaluation for head and neck proton therapy. J Appl Clin Med Phys 2022. https://doi.org/10.1002/acm2.13550.

[42] Hardcastle N, Tomé WA, Cannon DM, Brouwer CL, Wittendorp PW, Dogan N, et al. A multi-institution evaluation of deformable image registration algorithms for automatic organ delineation in adaptive head and neck radiotherapy. Radiat Oncol 2012;7:90. https://doi.org/10.1186/1748-717x-7-90.

[43] Schmitz HP, Rabe M, Janssens G, Bondesson D, Rit S, Parodi K, et al. Validation of proton dose calculation on scatter corrected 4D cone beam computed tomography using a porcine lung phantom. Phys Medicine Biology 2021. https://doi.org/10.1088/1361-6560/ac16e9.

[44] Pang B, Si H, Liu M, Fu W, Zeng Y, Liu H, et al. Comparison and evaluation of different deep learning models of synthetic CT generation from CBCT for nasopharynx cancer adaptive proton therapy. Méd Phys 2023;50:6920–30. https://doi.org/10.1002/mp.16777.

[45] Villarroel EB, Geets X, Sterpin E. Online adaptive dose restoration in intensity modulated proton therapy of lung cancer to account for inter-fractional density changes. Phys Imaging Radiat Oncol 2020;15:30–7. https://doi.org/10.1016/j.phro.2020.06.004.

[46] Ates O, Pirlepesov F, Uh J, Hua C, Merchant TE, Boria A, et al. Evaluating the impact of bowel gas variations for wilms' tumor in pediatric proton therapy. Cancers 2024;16:642. https://doi.org/10.3390/cancers16030642.